Supporting Information

Ion-exchange capacity (IEC)

The ion-exchange capacity (IEC) of the xerogels was determined using an acid-base titration method. Approximately 150 mg of each dried sample was immersed in 20 mL of sodium chloride solution (0.2 mol L^{-1}) for 48 hours to facilitate proton exchange. The liberated protons were then titrated with sodium hydroxide solution (C_0 = 0.02 mol L^{-1}) using phenolphthalein as the visual endpoint indicator. Each measurement was performed in triplicate, with the relative error maintained below 5%. The IEC value (mmol g^{-1}) was calculated according to Eq. (S1):

$$IEC = \frac{V_{(NaOH)} \times C_0}{W_{dry}} \quad (S1)$$

where V_{NaOH} and W_{dry} represented the consumed volume of NaOH solution (L), and the weight of the dry xerogel (g), respectively.

NH_3 temperature programmed (NH_3-TPD)

The NH_3 temperature-programmed desorption (NH_3-TPD) experiments were conducted using a TP-5076 TPD/TPR dynamic adsorption instrument. During the analysis, 100 mg of each sample was pretreated in an air flow (30 mL min^{-1}) at 393 K (ramp rate 12 K min^{-1}) for 1 hour, then cooled to 323 K under the same flow. The samples were subsequently exposed to 5% NH_3 (5 vol% NH_3 in He, flow rate: 30 mL min^{-1}) for 30 minutes. The physisorbed NH_3 was removed by flushing the sample with He (30 mL min^{-1}) for 30 minutes. Finally, the NH_3-TPD curves were recorded by heating the sample in He (30 mL min^{-1}) at a rate of 10 K/min from 323 to 623 K.

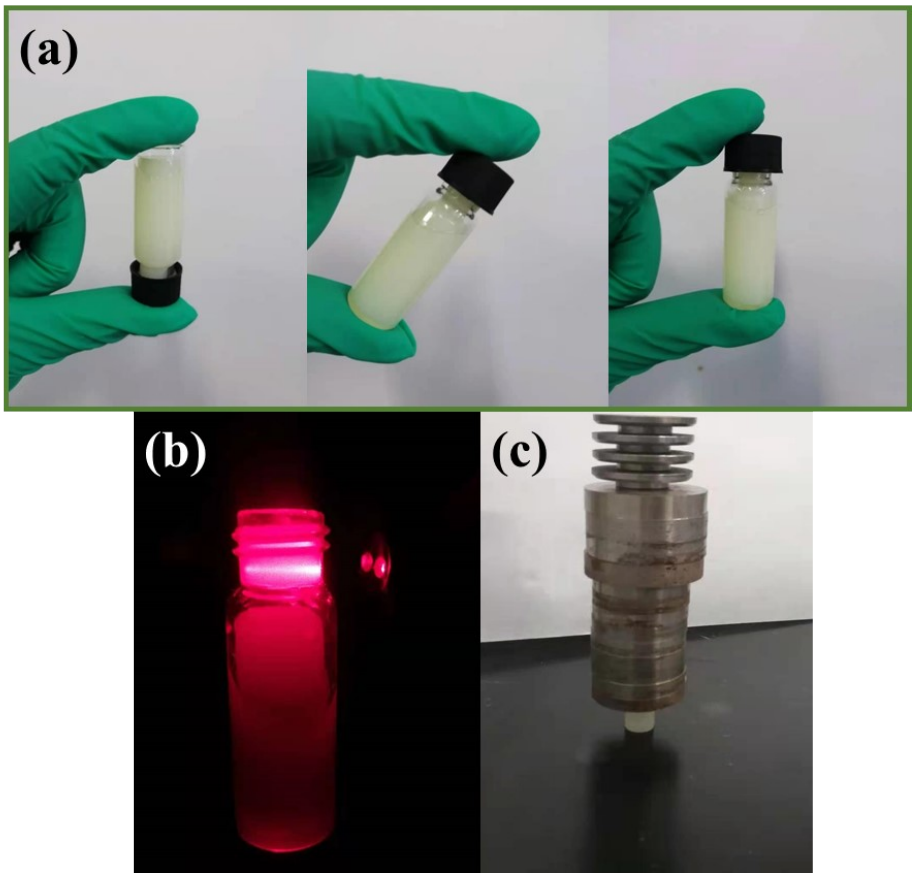

Fig. S1 (a) 'Non-flowing' gels and (b) Tyndall effect of Zr-FA-hydrogel; (c) the mechanical stability testing of Zr-FA-xerogel.

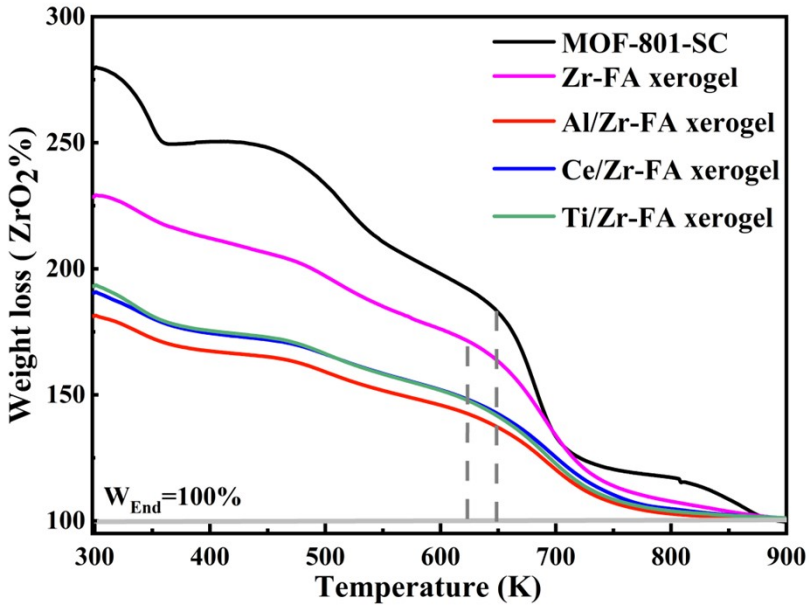

Fig. S2 TGA curves of MOF-801-SC, Zr-FA-xerogel and M/Zr-FA-xerogels.

For all curves, the ordinate axis was normalized to 100% for the solid residual at 1023 K, corresponding to ZrO_2 (grey horizontal line). The complete combustion reaction of perfect MOF-801 is as follows:

$$Zr_6O_6(Fum)_6(s) + O_2(g) \rightarrow 6ZrO_2(S) + 24CO_2(g) + 6H_2O(g)$$

The molar mass of perfect dehydroxylation $Zr_6O_6(Fum)_6$ is 1327 g mol^{-1}, and the complete conversion of dehydroxylation $Zr_6O_6(Fum)_6$ would yield $6ZrO_2$ solid residue. The molar mass of solid residue is $6\times M(ZrO_2) = 6\times 123.22 = 739.2$ g mol^{-1}.

$$\frac{\text{moles of } Zr_6O_6(Fum)_6}{\text{moles of } ZrO_2} = \frac{1}{6}$$

$$\text{moles of } Zr_6O_6(Fum)_6 = \frac{\text{moles of } ZrO_2}{6}$$

$$Wt_{\text{perfect plat}} = \left(\frac{MW_{Zr_6O_6(Fum)_6}}{6 \times MW_{ZrO_2}}\right) = \frac{1372}{6 \times 123.22} = 1.795$$

The perfect platform of $Zr_6O_6(Fum)_6$ should be found at 179.5% on the TG trace normalized to 100% solid residue. Through the TG curve, the experimental platform ($W_{exp.plat}$) of Zr-FA-xerogel-0.04 was found to be 148.8% (as highlighted by the grey dashed line, T_{plat} = 368 K), which is obviously smaller than $Wt_{perfect\ plat}$ (179.5%), indicating that defects existed in the material. For the idealized defect-free MOF-801-SC formula (Zr_6O_6(fumarate)$_6$), the theoretical weight loss from ligand combustion is 50.1%. The solvent was removed to calculate the number of ligand defects. The general dehydroxylated formula is $Zr_6O_{12-x}(Fum)_x$, and the number of ligands was calculated according to the following formula:

$$MW_{defected} = 547.2 + 192 + 98X = 739.2 + 98X$$

$$W_{exp.plat} \times 739.2 = 739.2 + 98X$$

$$X = \frac{(W_{exp.plat} - 1)\times 739.2}{98} = (W_{exp.plat} - 1)\times 7.54$$

$$X = (159.8\% - 1)\times 7.54 = 4.51$$

Therefore, the formula of desolvated and dehydroxylated Ti/Zr-FA-xerogel is $Zr_6O_4(OH)_{6.00}$(fumarate)$_{4.00}$.

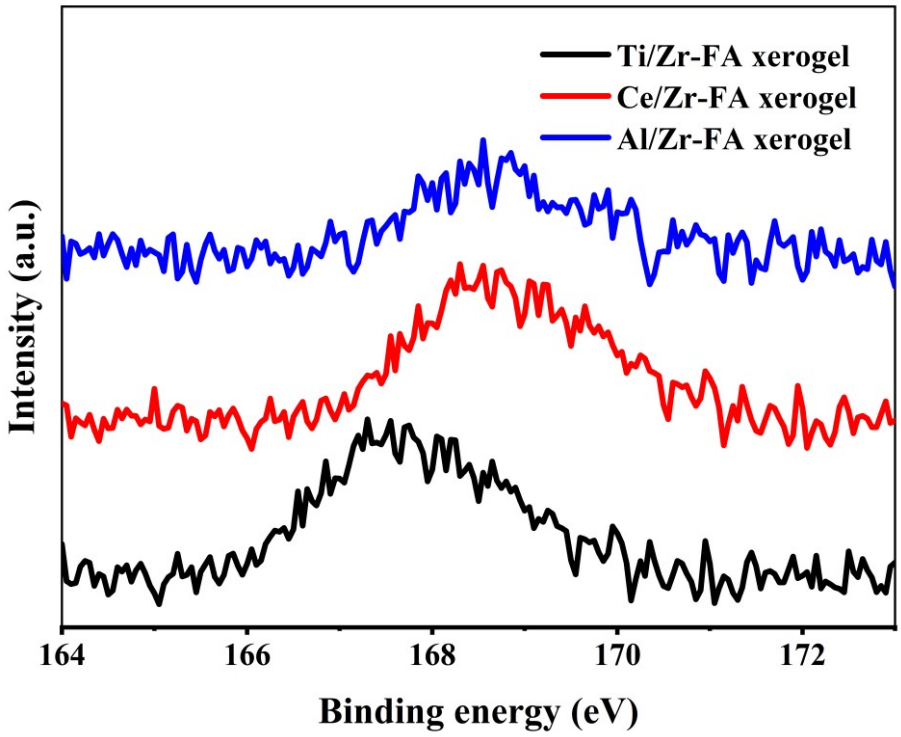

Fig. S3 S 2p XPS spectra of M/Zr-FA-xerogels.

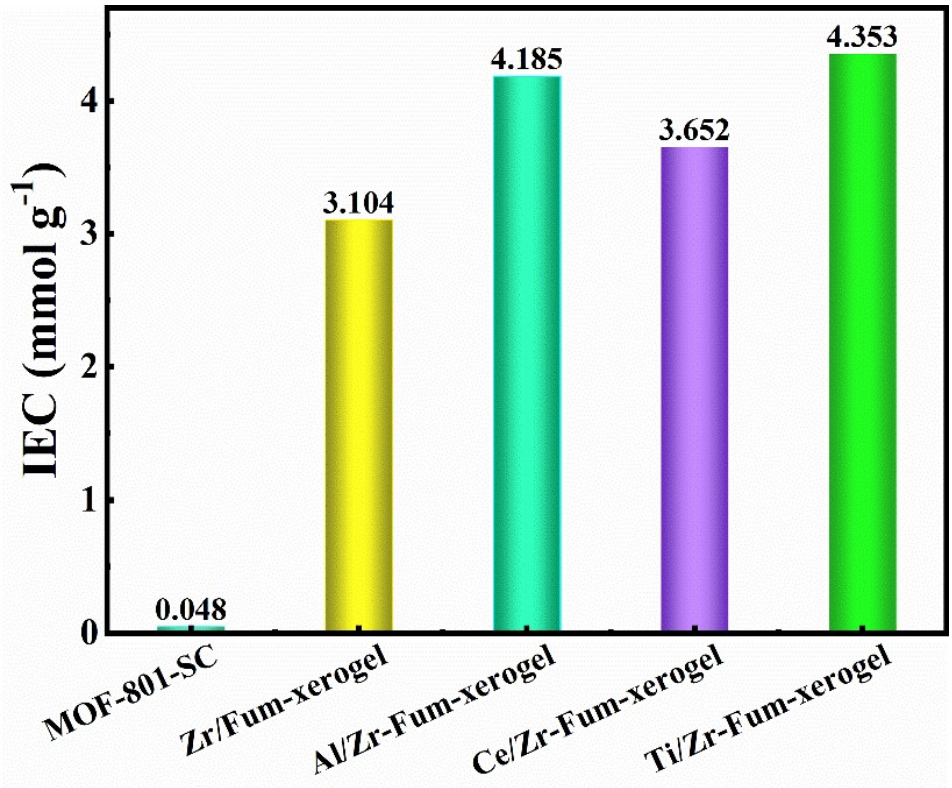

Fig. S4 IEC values of MOF-801-SC and xerogels.

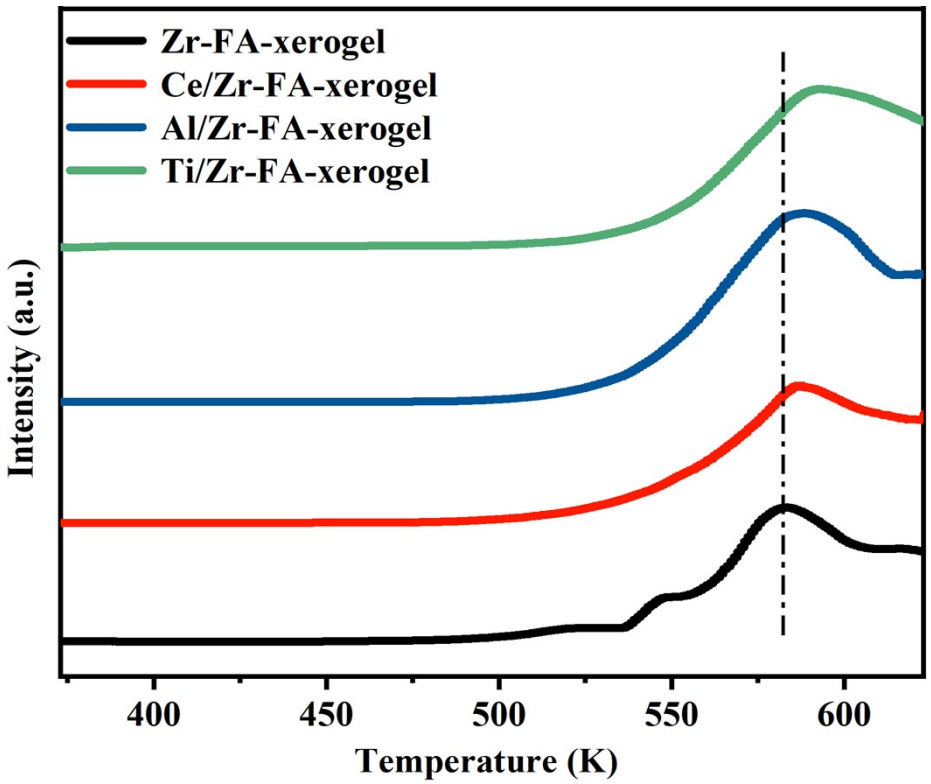

Fig. S5 NH_3 temperature programmed (NH_3-TPD) curves of Zr-FA-xerogel and M/Zr-FA-xerogels.

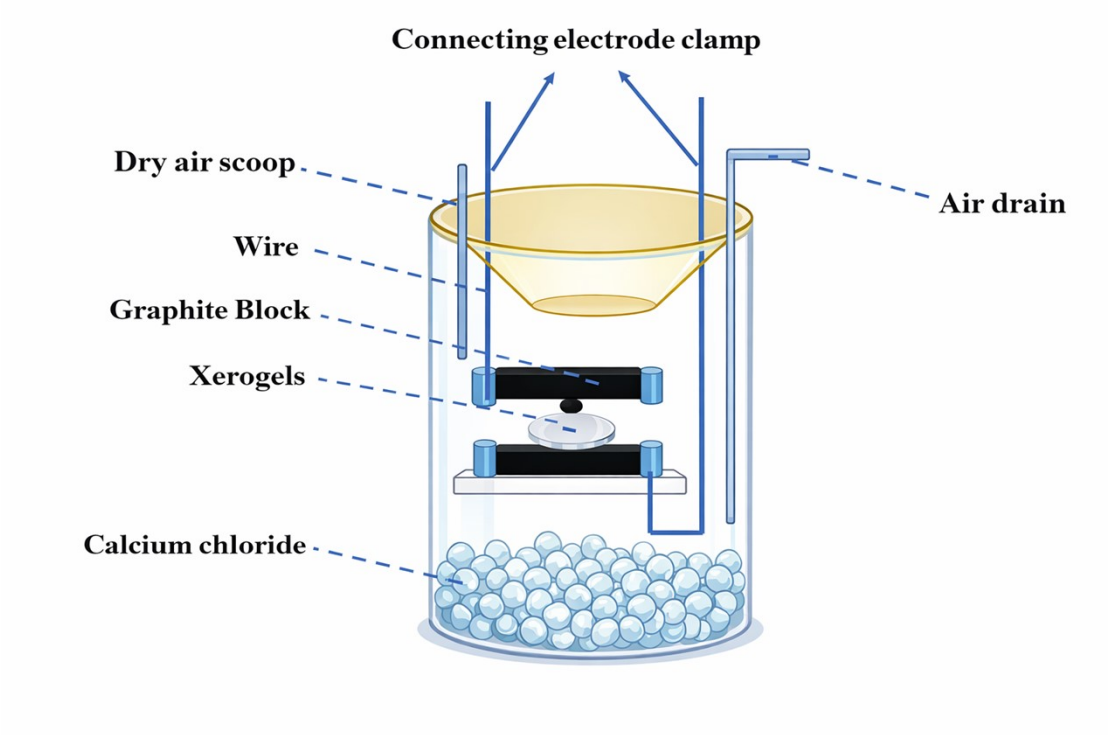

Fig. S6 The home-made device of the EIS measurements.

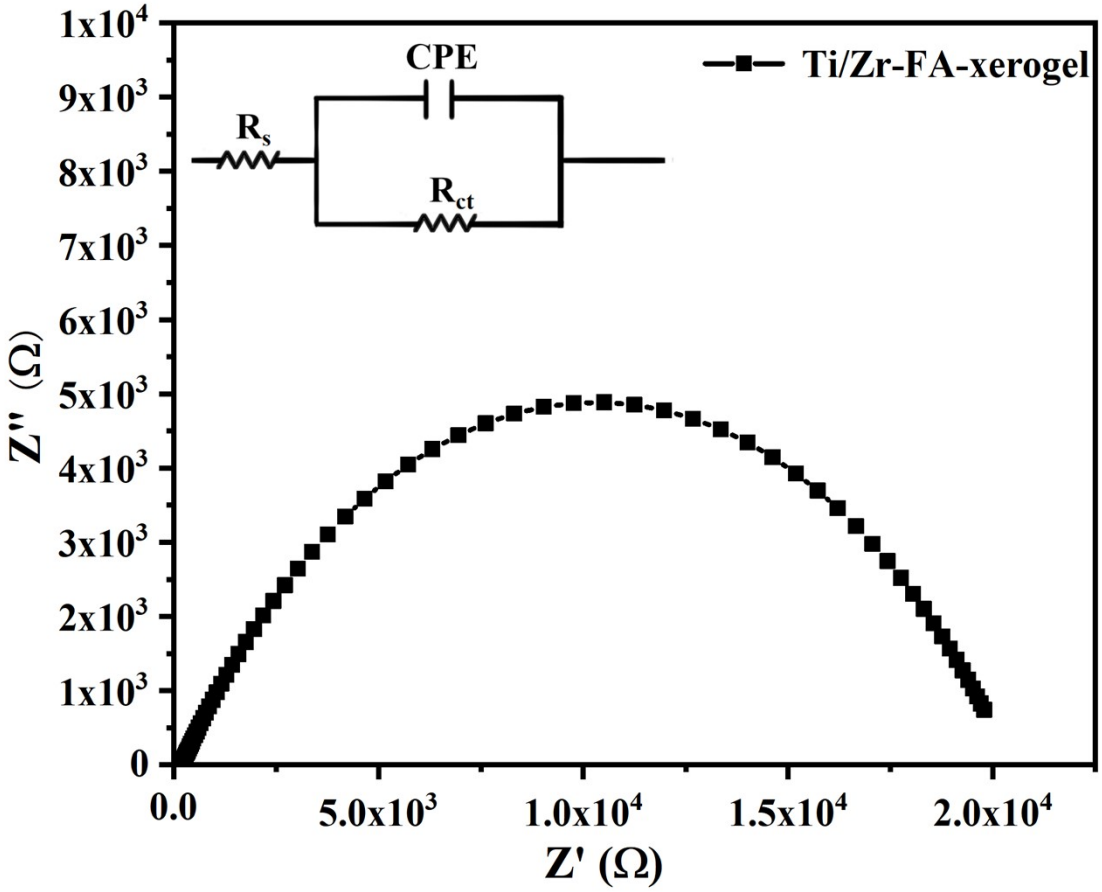

Fig. S7 EIS fitting circuit of Ti/Zr-FA-xerogel.

Table S1 Pore structural parameters for M/Zr-FA-xerogels and MOF-801-SC.

Materials	S_{BET} (m^2 g^{-1})	Pore volume (cm^3 g^{-1})	Pore width (nm)
MOF-801-SC	646	0.515	0.8, 1.0, 2.6
Zr-FA-xerogel	416	0.397	0.8, 6.6
Al/Zr-FA-xerogel	449	0.492	0.12, 0.48, 6.3
Ce/Zr-FA-xerogel	508	0.811	0.36, 0.8, 9.4
Ti/Zr-FA-xerogel	458	0.536	0.12, 0.52, 7.0

Table S2 The number of ligands per formula unit in Zr-FA-xerogel, M/Zr-FA-xerogels and MOF-801-SC according to TGA.

Materials	$W_{exp.plat}$ (%)	Number of ligands per SUB(x)	Number of missing-linker per SUB(6-x)	The concentration of missing-linker defects (=(6-x)/6)×100%)
MOF-801-SC	184.2	6.34	/	/
Zr-FA-xerogel	172.3	5.45	0.55	9.2
Al/Zr-FA-xerogel	147.0	3.54	2.46	41.0
Ce/Zr-FA-xerogel	153.1	3.99	2.01	33.5
Ti/Zr-FA-xerogel	153.0	4.00	2.00	33.3

Table S3 Spectral fitting results of O 1s for M/Zr-FA-xerogels.

Materials	Zr–O–Zr (% Area)	Zr−μ_3-OH (% Area)	Zr−μ_1-OH& R–COO^- (% Area)
Zr-FA-xerogel	8.2%	33.3%	58.5%
Al/Zr-FA-xerogel	20.1%	44.5%	35.4%
Ce//Zr-FA-xerogel	14.8%	38.7%	46.5%
Ti/Zr-FA-xerogel	19.9%	40.7%	39.4%

Table S4 Spectral fitting results of Zr 3d for M/Zr-FA-xerogels.

MOFs	Zr−O−Zr/Zr–COO-R (% Area)	Zr−OH (defect) (% Area)
Zr-FA-xerogel	52.42	47.58
Al/Zr-FA-xerogel	46.79	53.21
Ce/Zr-FA-xerogel	50.7	49.3
Ti/Zr-FA-xerogel	49.55	50.45

Table S5 Proton conductivities of MOFs under anhydrous condition.

Compounds	Proton conductivity (S cm^{-1})			Reference
	Min (K)	Max (K)	Temp range (K)	
His@Zn-MOF-74		4.3×10^{-9}	313-419	[1]
$[Co_2Na(bptc)_2][Emim]_3$	3.89×10^{-8}	6.33×10^{-7}	343-443	[2]
$(NH_4)_2[ZrF_2(HPO_4)_2]$	1.18×10^{-7}	1.1×10^{-5}	363-503	[3]
In-IA-2D-2	2.33×10^{-5}	2.72×10^{-5}	298-363	[4]
$[Zn(H_2PO_4)_2(HPO_4)]\cdot H_2dabco$	8.48×10^{-10}	8×10^{-5}	363-433	[5]
FJU-31@Ch	1.17×10^{-6}	8.05×10^{-5}	231-393	[6]
$\{[(Me_2NH_2)_3(SO_4)]_2[Zn_2(ox)_3]\}_n$	7×10^{-5}	1×10^{-4}	303-423	[7]
$[Zn(H_2PO_4)_2(TzH)_2]n$	1.56×10^{-5}	1.2×10^{-4}	318-423	[8]
$[Zn(H_2PO_4)_2(HPO_4)]\cdot(H_2dmbim)_2$	1.22×10^{-9}	2×10^{-4}	303-463	[5]
β-$PCMOF_2(Tz)_{0.3}$	1.04×10^{-6}	2×10^{-4}	296-423	[6]
$[Zn(HPO_4)(H_2PO_4)_2](ImH_2)_2$	4.71×10^{-8}	2.6×10^{-4}	298-403	[9]
FJU-31@Hq	1.49×10^{-5}	2.65×10^{-4}	233-398	[6]
$(Me_2NH_2)[Eu(L)]$	1.69×10^{-4}	1.25×10^{-3}	303-423	[10]
$[Zn_3(H_2PO_4)_6](H_2O)_3(Hbim)$	1.4×10^{-7}	1.3×10^{-3}	303-393	[11]
EMIMCl@UiO-67	1.52×10^{-4}	1.67×10^{-3}	373-473	[12]
$His@[Al(OH)(1,4\text{-}ndc)]_n$	3×10^{-5}	1.7×10^{-3}	298-423	[13]
$[Eu_2(CO_3)(ox)_2(H_2O)_2]\cdot4H_2O$	9.48×10^{-6}	2.08×10^{-3}	298-423	[14]
PA@MIL-101	2.5×10^{-4}	3×10^{-3}	313-423	[15]
Im@IEF-11-100	7.03×10^{-5}	3.08×10^{-3}	313-393	[16]
FJU-17	2.9×10^{-6}	1.08×10^{-2}	233-373	[17]
Im@MC-32	1.14×10^{-5}	1.4×10^{-2}	323-393	[18]
Zr/BTC-xerogels-TMSA	9×10^{-4}	1.4×10^{-2}	253-363	[19]
FJU-106	6.45×10^{-4}	1.8×10^{-2}	253-343	[20]
Zr/Fum-xerogel-0.04	5.68×10^{-4}	2.5×10^{-2}	233-433	[21]
Ti/Zr-FA-xerogel	1.9×10^{-3}	5×10^{-2}	233-433	This work

Reference

[1] M. Inukai, S. Horike, D. Umeyama, Y. Hijikata, S. Kitagawa, Investigation of post-grafted groups of a porous coordination polymer and its proton conduction behavior, Dalton Transactions 41(43) (2012).

[2] W.-X. Chen, H.-R. Xu, G.-L. Zhuang, L.-S. Long, R.-B. Huang, L.-S. Zheng, Temperature-dependent conductivity of Emim+ (Emim+ = 1-ethyl-3-methyl imidazolium) confined in channels of a metal–organic framework, Chemical Communications 47(43) (2011).

[3] D. Gui, T. Zheng, J. Xie, Y. Cai, Y. Wang, L. Chen, J. Diwu, Z. Chai, S. Wang, Significantly Dense Two-Dimensional Hydrogen-Bond Network in a Layered Zirconium Phosphate Leading to High Proton Conductivities in Both Water-Assisted Low-Temperature and Anhydrous Intermediate-Temperature Regions, Inorganic Chemistry 55(24) (2016) 12508-12511.

[4] T. Panda, R. Banerjee, High Charge Carrier Mobility in Two Dimensional Indium (III) Isophthalic Acid Based Frameworks, Proceedings of the National Academy of Sciences, India Section A: Physical Sciences 84(2) (2014) 331-336.

[5] M. Inukai, S. Horike, W. Chen, D. Umeyama, T. Itakura, S. Kitagawa, Template-directed proton conduction pathways in a coordination framework, J. Mater. Chem. A 2(27) (2014) 10404-10409.

[6] Y. Ye, X. Wu, Z. Yao, L. Wu, Z. Cai, L. Wang, X. Ma, Q.-H. Chen, Z. Zhang, S. Xiang, Metal–organic frameworks with a large breathing effect to host hydroxyl compounds for high anhydrous proton conductivity over a wide temperature range from subzero to 125 °C, Journal of Materials Chemistry A 4(11) (2016) 4062-4070.

[7] S.S. Nagarkar, S.M. Unni, A. Sharma, S. Kurungot, S.K. Ghosh, Two-in-One: Inherent Anhydrous and Water-Assisted High Proton Conduction in a 3D Metal–Organic Framework, Angewandte Chemie International Edition 53(10) (2013) 2638-2642.

[8] S. Bureekaew, S. Horike, M. Higuchi, M. Mizuno, T. Kawamura, D. Tanaka, N. Yanai, S. Kitagawa, One-dimensional imidazole aggregate in aluminium porous coordination polymers with high proton conductivity, Nature Materials 8(10) (2009) 831-836.

[9] S. Horike, D. Umeyama, M. Inukai, T. Itakura, S. Kitagawa, Coordination-Network-Based Ionic Plastic Crystal for Anhydrous Proton Conductivity, Journal of the American Chemical Society 134(18) (2012) 7612-7615.

[10] D. Zhang, G. Li, Y. Peng, L. Li, Synthesis of a Ternary Thiostannate with 3D Channel Decorated by Hydronium for High Proton Conductivity, Inorganic Chemistry 56(1) (2016) 208-212.

[11] D. Umeyama, S. Horike, M. Inukai, T. Itakura, S. Kitagawa, Inherent Proton Conduction in a 2D Coordination Framework, Journal of the American Chemical Society 134(30) (2012) 12780-12785.

[12] L.-H. Chen, B.-B. Wu, H.-X. Zhao, L.-S. Long, L.-S. Zheng, High temperature ionic conduction mediated by ionic liquid incorporated within the metal-organic framework UiO-67(Zr), Inorganic Chemistry Communications 81 (2017) 1-4.

[13] D. Umeyama, S. Horike, M. Inukai, Y. Hijikata, S. Kitagawa, Confinement of Mobile Histamine in Coordination Nanochannels for Fast Proton Transfer, Angewandte Chemie International Edition 50(49) (2011) 11706-11709.

[14] Y. Zhou, J. Yang, H. Su, J. Zeng, S.P. Jiang, W.A. Goddard, Insight into Proton Transfer in Phosphotungstic Acid Functionalized Mesoporous Silica-Based Proton Exchange Membrane Fuel Cells, Journal of the American Chemical Society 136(13) (2014) 4954-4964.

[15] V.G. Ponomareva, K.A. Kovalenko, A.P. Chupakhin, D.N. Dybtsev, E.S. Shutova, V.P. Fedin, Imparting High Proton Conductivity to a Metal–Organic Framework Material by Controlled Acid Impregnation, Journal of the American Chemical Society 134(38) (2012) 15640-15643.

[16] J.-X. Qu, Y.-M. Fu, X. Meng, Y.-O. He, H.-X. Sun, R.-g. Yang, H.-N. Wang, Z.-M. Su, A porous Ti-based metal–organic framework for CO2photoreduction and imidazole-dependent anhydrous proton conduction, Chemical Communications 59(8) (2023) 1070-1073.

[17] L. Liu, Z. Yao, Y. Ye, Q. Lin, S. Chen, Z. Zhang, S. Xiang, Enhanced Intrinsic Proton Conductivity of Metal–Organic Frameworks by Tuning the Degree of Interpenetration, Crystal Growth & Design 18(7) (2018) 3724-3728.

[18] S. Liu, H. Li, Y. Shuai, Z. Ding, Y. Liu, Imidazole encapsulated in core–shell MOF@COFs with a high anhydrous proton conductivity, Materials Advances 3(23) (2022) 8647-8655.

[19] D. Gao, J. Tang, F. Zhang, C. Wen, L. Feng, C. Wan, F. Qu, X. Liang, Modulation of defects in metal organic gels to enhance anhydrous proton conduction from subzero to moderate temperature, J. Colloid Interface Sci. 650 (2023) 19-27.

[20] Q. Lin, Y. Ye, L. Liu, Z. Yao, Z. Li, L. Wang, C. Liu, Z. Zhang, S. Xiang, High proton conductivity in metalloring-cluster based metal-organic nanotubes, Nano Research 14(2) (2020) 387-

391.

[21] J. Tang, F. Zhang, X. Liang, G. Dai, F. Qu, Abundant defects of zirconium-organic xerogels: High anhydrous proton conductivities over a wide temperature range and formic acid impedance sensing, Journal of Colloid and Interface Science 607 (2022) 181-191.